

Unifying susceptible-infected-recovered processes on networks

Lucas Böttcher^{1,2,3} and Nino Antulov-Fantulin⁴

¹*Computational Medicine, UCLA, 90095-1766, Los Angeles, United States*

²*Institute for Theoretical Physics, ETH Zurich, 8093, Zurich, Switzerland*

³*Center of Economic Research, ETH Zurich, 8092, Zurich, Switzerland**

⁴*Computational Social Science, ETH Zurich, 8092, Zurich, Switzerland†*

(Dated: May 10, 2022)

Waiting times between two consecutive infection and recovery events in spreading processes are often assumed to be exponentially distributed, which results in Markovian (i.e., memoryless) continuous spreading dynamics. However, this is not taking into account memory (correlation) effects and discrete interactions that have been identified as relevant in social, transportation, and disease dynamics. We introduce a novel framework to model (non-)Markovian susceptible-infected-recovered (SIR) stochastic processes that are evolving either in continuous or discrete time on networks. We apply our simulation framework to study hybrid SIR processes that describe infections as discrete-time Markovian and recovery events as continuous-time non-Markovian processes, which mimic the distribution of cell-cycle times. Our results suggest that the effective-spreading-rate description of epidemic processes fails to uniquely capture the behavior of such hybrid and also general non-Markovian disease dynamics. Providing a unifying description of general Markovian and non-Markovian disease outbreaks, we instead show that the mean transmissibility produces the same phase diagrams independent of the underlying inter-event-time distributions.

Introduction. Models of epidemic processes such as the *susceptible-infected-recovered* (SIR) model and related models provided various insights into dynamical and stationary features of disease, opinion, and failure spread in social and technical systems [1–3]. In the SIR model, infected individuals may transmit a disease to susceptible ones. After a certain period, infected individuals recover and are not part of the disease-transmission process anymore. The exact time evolution of the continuous-time stochastic SIR spreading process is described by the Chapman-Kolmogorov equation or its differential form (i.e., the master equation). However, exact analytical solutions of the master equation are limited to special cases and therefore different approximations are being used (e.g., deterministic ODE models [4–6] and cavity-like models [7, 8]). Gillespie and *kinetic Monte-Carlo* (kMC) approaches [9] provide techniques to generate statistically exact trajectories of a master equation. The assumption underlying kMC methods is that waiting times between consecutive recovery and infection events are exponentially distributed. However, many natural processes including social dynamics [10, 11] exhibit correlation and memory (i.e., non-Markovian) effects [12] and are therefore not described by exponential (i.e., memoryless) waiting-time distributions [13]. Recent attempts to simulate non-Markovian disease dynamics led to the development of the *non-Markovian Gillespie algorithm* (nMGA) [14] and the *Laplace Gillespie algorithm* (LGA) [15]. Both methods are based on a mapping of multiple stochastic processes with general (continuous) waiting-time distributions to a modified kMC algorithm. The nMGA is only exact for a sufficiently large number of processes and requires to re-calculate all individual rates at every time step. The LGA interprets survival functions of waiting-time distributions as Laplace trans-

forms of underlying event-rate distributions. Although the LGA is exact for arbitrary numbers of processes, it is only applicable to certain waiting-time distributions [15].

In this Letter, we develop a novel framework to simulate non-Markovian SIR processes with general discrete and continuous waiting-time distributions. Our framework is based on a mapping of waiting times to a shortest-path problem in a weighted spreading network. We use our framework to study hybrid continuous-discrete SIR (henceforth *hybrid SIR*) processes. Discrete Markovian and non-Markovian infection processes account for latency intervals during which no infection events occur or the discrete nature of social interactions (e.g., meetings, bus rides, flights, etc.) and are considered to be more closely aligned with corresponding empirical data than their continuous counterparts [16–18]. Continuous-time infection processes neglect such latency periods that may arise from incubation periods (e.g., 8-14 days for measles [19]) and finite transfer times of information in communication and transportation networks. Our results suggest that hybrid and also general non-Markovian disease outbreaks cannot be uniquely captured by effective spreading rates. However, by mapping such SIR processes to bond percolation [20, 21], we show that the corresponding mean transmissibilities produce the same phase diagrams independent of the underlying infection- and recovery-time distributions; thus providing a unifying description of general Markovian and non-Markovian SIR processes. The framework we propose assumes no specific form of waiting-time distributions [17, 22] and allows us to simulate and analytically describe general discrete, continuous, and hybrid variants of Markovian and non-Markovian SIR dynamics.

Shortest-path (SP) kMC. Before focusing on the simulation of hybrid SIR dynamics, we introduce the neces-

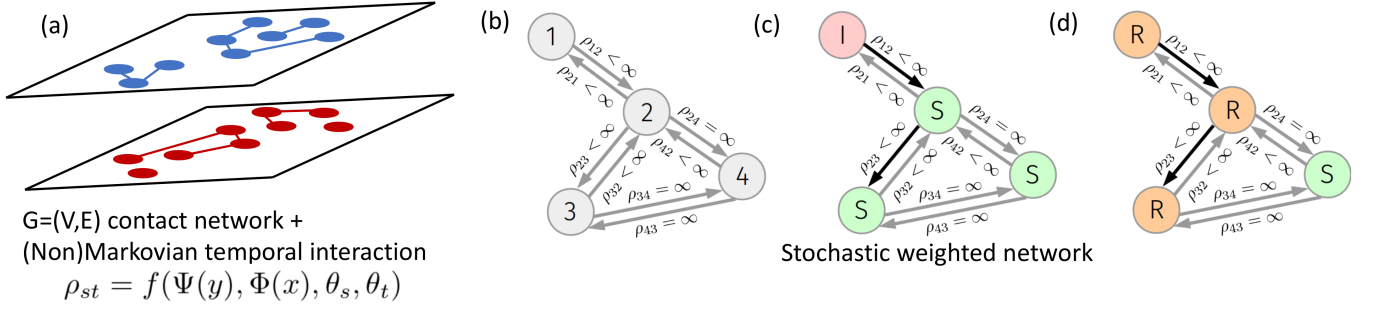


Figure 1. **SIR dynamics on a spreading network.** (a) Contact network as a projection of multiplex network of households, workplaces, communities, etc. and (non-)Markovian temporal interaction per edge $\rho_{st} = f(\Psi(y), \Phi(x), \theta_s, \theta_t)$, with demographic, social or intervention factors θ_s, θ_t . (b) Initialization of edge weights according to Eq. (1) in a spreading network that consists of 4 nodes. Finite edge weights indicate that disease transmission can occur along the corresponding edge. (c) Node 1 is infected and transmits the disease to nodes 2 and 3 that are connected via paths of finite length (indicated by black arrows). The times at which nodes 2 and 3 get infected are ρ_{12} and $\rho_{12} + \rho_{23}$. (d) After determining all possible infections in the spreading network, infected nodes are considered to be recovered in the long-time limit $\tau \rightarrow \infty$.

sary mathematical toolbox that allows us to map general waiting times to a shortest-path problem in an underlying spreading network. Let $\phi(\tau)$ and $\psi(\tau)$ be the probability-density or probability mass functions (PDFs or PMFs) of recovery and infection times. In continuous time, the probability that a recovery (infection) event occurs in the interval $(\tau, \tau + d\tau)$ is $\phi(\tau) d\tau$ ($\psi(\tau) d\tau$). The discrete time analogues $\phi(\tau)$ and $\psi(\tau)$ are the recovery and infection probabilities after $\lfloor \tau \rfloor$ steps, where $\lfloor \cdot \rfloor$ denotes the floor function. We denote the cumulative distribution function (CDF) of $\phi(\tau)$ and $\psi(\tau)$ by $\Phi(\tau)$ and $\Psi(\tau)$. The function $\Phi(\tau)$ ($\Psi(\tau)$) is the probability that a recovery (infection) event occurred in $[0, \tau]$. In the case of Poissonian SIR dynamics, waiting-time distributions are described by the PDFs $\phi(\tau) = \gamma e^{-\gamma\tau}$ and $\psi(\tau) = \beta e^{-\beta\tau}$ and CDFs $\Phi(\tau) = 1 - e^{-\gamma\tau}$ and $\Psi(\tau) = 1 - e^{-\beta\tau}$, where γ and β are the corresponding recovery and infection rates. Note that we use prefixes such as “Erlang-geometric” to indicate the recovery and infection time distributions ($\phi(\tau)$ and $\psi(\tau)$) of the corresponding hybrid SIR process.

For given distributions $\phi(\tau)$ and $\psi(\tau)$, we consider M realizations of SIR dynamics to correspond to an ensemble of M directed spreading networks $\{G_k(V, E)\}_{k \in \{1, \dots, M\}}$, where V and E denote the sets of nodes and edges. Each network $G_k(V, E)$ is initialized as follows. For each node s in $G_k(V, E)$, we generate a random number $x \sim \mathcal{U}(0, 1)$ and use an inverse transform sampling of $\Phi(\tau)$ to determine the recovery time of node s according to $\Phi^{-1}(x)$. For each node t that is adjacent to s , we generate another random number $y \sim \mathcal{U}(0, 1)$ and determine the infection time $\Psi^{-1}(y)$. We now use $\Phi^{-1}(x)$ and $\Psi^{-1}(y)$ to determine edge weights [23]

$$\rho_{st} = \begin{cases} \Psi^{-1}(y), & \Psi^{-1}(y) \leq \Phi^{-1}(x), \\ \infty, & \Psi^{-1}(y) > \Phi^{-1}(x). \end{cases} \quad (1)$$

We set ρ_{st} to $\Psi^{-1}(y)$ (i.e., the disease transmission time from node s to t) if infection occurs before recovery, and

$\rho_{st} = \infty$ otherwise. Note that the interaction terms can also be general $\rho_{st} = f(\Psi(y), \Phi(x), \theta_s, \theta_t)$, where $f(\cdot)$ accounts for node-dependent transmission features (θ_s, θ_t) like age, gender, and other social and demographic factors including interventions like the probability of quarantine or contact containment restrictions (see Fig. 1 (a)). If the CDFs are not invertible, we can generate edge weights with rejection sampling. In Fig. 1 (b), we show an illustration of the weight initialization procedure for a network that consists of 4 nodes. We again note that networks $G_k(V, E)$ are directed (i.e., weights ρ_{st} may be different from ρ_{ts}). In the case of a Poissonian dynamics, we obtain

$$\rho_{st} = \begin{cases} -\frac{\ln(x)}{\beta}, & -\frac{\ln(x)}{\beta} \leq -\frac{\ln(y)}{\gamma}, \\ \infty, & -\frac{\ln(x)}{\beta} > -\frac{\ln(y)}{\gamma}. \end{cases} \quad (2)$$

In addition to edge weights, we also keep track of node weights $\tau_i = \Phi^{-1}(x)$ to describe the evolution of SIR dynamics in a network. The network $G(V, E)$ can be a projection of multiplex networks [24] with workplace-, household-, and community layers.

After having identified all weights, we obtain one realization $G_k(V, E)$ of the spreading network. In the next step, we take $G_k(V, E)$ and infect one uniformly at random selected node (see Fig. 1 (c)). All nodes that are connected to the initially infected node through paths of finite length are also infected and eventually recover in the limit of $\tau \rightarrow \infty$ (see Fig. 1 (d)). The shortest-path length between an infected source and its target node is the corresponding disease transmission time, which can be viewed as a “least action principle” for kMC. If all paths that connect two nodes are infinite, we know that one or multiple recovered nodes hinder the disease transmission (see node 4 in Fig. 1). To describe SIR dynamics with N initially infected nodes, we use I_k^j to denote the set of infected nodes that result from an initial infection of node j in $G_k(V, E)$. The corresponding set of all in-

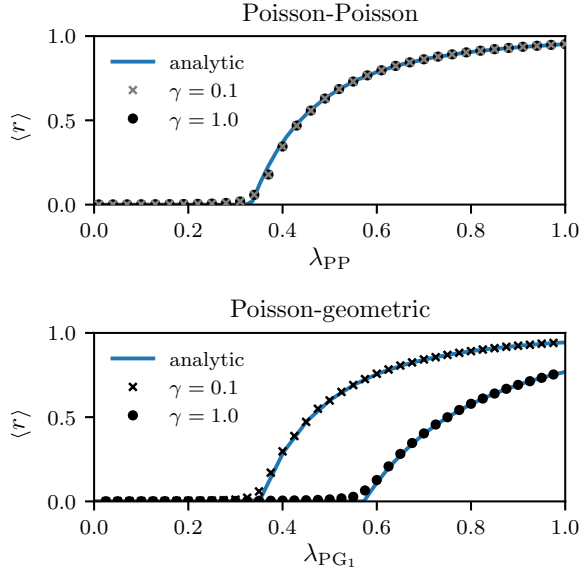


Figure 2. **Fraction of recovered in Poissonian and hybrid Poisson-geometric SIR processes.** In the top panel, we show the fraction of recovered nodes $\langle r \rangle$ (see Eq. (3)) as a function of the effective spreading rate $\lambda_{PP} = \beta/\gamma$ for fully Poissonian SIR processes; and in the bottom panel we show the dependence of $\langle r \rangle$ on $\lambda_{PG_1} = q/\gamma$. Analytical solutions (blue solid lines) are based on Eqs. (10) and (11) for a random-regular graph with $k = 5$. Numerical simulations have been performed for $N = 10^5$ nodes and $M = 10^2$ realizations.

fectured nodes that result from multiple spreading seeds in $G_k(V, E)$ is $I_k = \bigcup_{j=1}^N I_k^j$ (see *Supplemental Information* (SI) for further details). Infection times can be monitored by keeping track of the individual shortest-path lengths. The stationary fraction of recovered nodes in network $G_k(E, V)$ is $r_k = |I_k|/N$, where $N = |V|$ is the number of nodes, and the corresponding ensemble average over $\{G_k(V, E)\}_{k \in \{1, \dots, M\}}$ yields

$$\langle r \rangle = \frac{1}{M} \sum_{k=1}^M r_k. \quad (3)$$

For each network realization $G_k(E, V)$, we have to identify the shortest paths, an operation of computational complexity of order $\mathcal{O}(|E| + |V| \log |V|)$ [25]. In the SI, we consider Poissonian dynamics (see Eq. (2)) and show that our SP-kMC simulations of stationary and dynamical SIR features agree well with corresponding kMC simulations. An advantage of our proposed shortest-path SIR simulation method is the possibility to simulate general Markovian and non-Markovian dynamics with continuous and discrete waiting time distributions.

Hybrid continuous-discrete SIR dynamics. To describe latency periods in infection processes (i.e., no infection occurs during a certain time window), we apply our simulation framework to hybrid Poisson-geometric SIR dynamics with discrete infection events that are dis-

tributed according to a geometric density function

$$\psi_{G_1}(\tau) = \sum_{k=1}^{\infty} \delta(\tau - k)(1 - q)^{k-1}q, \quad (4)$$

where q is the probability that an infection event occurs within a time step of 1 and $\delta(\cdot)$ is the Dirac delta function. In the SI, we also consider an alternative definition of the geometric distribution ψ_{G_2} that takes on finite values for all non-negative integers and show that the master equation of hybrid Poisson-geometric SIR dynamics is no longer time-homogeneous. The geometric distribution is the discrete memoryless counterpart of exponential distributions. We can now use our simulation framework to study disease outbreak characteristics of such hybrid SIR processes. As for many epidemic processes [5], we characterize disease dynamics in terms of the effective spreading rate $\lambda = \langle \tau \rangle_{\phi} / \langle \tau \rangle_{\psi}$, where $\langle \tau \rangle_{\psi}$ and $\langle \tau \rangle_{\phi}$ are the mean times to infection and recovery, respectively. For fully a Poissonian SIR process, the effective spreading rate is $\lambda_{PP} = \beta/\gamma$ and invariant upon rescaling of infection and recovery rates by a constant factor. That is, the corresponding fraction of recovered (see Eq. (3)) only depends on the effective spreading rate λ_{PP} (see Fig. 2 (top)). By analogy, we now use $\lambda_{PG_1} = 1/(\gamma \langle \tau \rangle_{\psi})$ to denote the effective spreading rate for Poissonian-geometric dynamics with infection-time PDF ψ_{G_1} and

$$\langle \tau \rangle_{\psi} = \sum_{\tau'=1}^{\infty} \tau' (1 - q)^{\tau'-1} q = q^{-1}. \quad (5)$$

However, unlike in fully Poissonian SIR dynamics, we cannot uniquely capture the corresponding phase space by the effective spreading rate λ_{PG_1} (see Fig. 2 (bottom)). That is, we observe different fractions of recovered $\langle r \rangle$ for the same value of λ_{PG_1} . To better understand the phase space of hybrid SIR processes, we proceed with a mapping to bond percolation.

Mapping hybrid SIR dynamics to bond percolation. We now analytically characterize the hybrid SIR disease prevalence in terms of the mean transmissibility \bar{T} that describes the probability of an infection to be transmitted from an infected to an adjacent susceptible node [21]:

$$\bar{T} = \int_0^{\infty} \phi(\tau) \int_0^{\tau} \psi(\tau') d\tau' d\tau. \quad (6)$$

In networks with no degree correlations, the critical transmissibility above which an SIR epidemic spreads through a finite fraction of the system is given by the bond percolation threshold [1, 21]

$$p_c = \frac{\langle k \rangle}{\langle k^2 \rangle - \langle k \rangle}, \quad (7)$$

where $\langle k \rangle$ and $\langle k^2 \rangle$ denote the first and second moment of the degree distribution P_k . For a Poisson-geometric

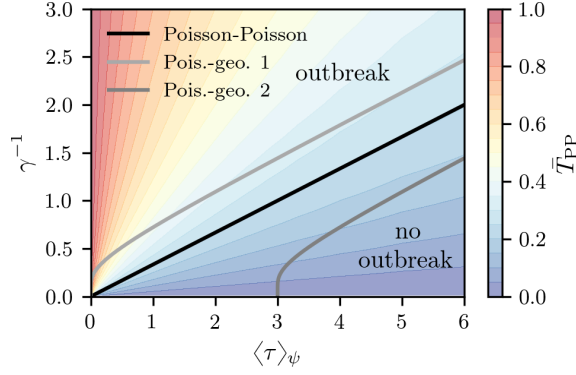


Figure 3. **Comparison of phase spaces.** We show the separation lines between phases with and without disease outbreaks. The black solid line corresponds to Poissonian SIR dynamics with $T_{PP} = \lambda_{PP}/(1 + \lambda_{PP})$ and $\lambda_{PP} = \beta/\gamma$. The light (dark) grey solid line describes the phase separation for Poissonian-geometric SIR dynamics with ψ_{G_1} (ψ_{G_2}) (see Eqs. (4) and (8) and the SI for details).

SIR dynamics, the mean transmissibility is

$$\bar{T}_{PG_1} = \bar{T}_{PG_1}(\gamma, q) = e^{-\gamma} \left[1 + \frac{(e^\gamma - 1)(q - 1)}{e^\gamma + q - 1} \right]. \quad (8)$$

In the SI, we provide further details about the derivation of Eq. (8) and provide a comparison between the fully Poissonian and the Poissonian-geometric case. According to Eqs. (7) and (8), we find the phase separation line $q_c = p_c(e^\gamma - 1)/(1 - p_c)$, which separates the phases with and without disease outbreaks (see Fig. 3). For $\gamma = 1$ and $\gamma = 0.1$, we obtain the critical effective spreading rates $\lambda_{PG_1}^c \approx 0.57$ and $\lambda_{PG_1}^c \approx 0.35$, respectively. These values agree well with the numerical data of Fig. 2 (bottom).

Note that $\bar{T}_{PG_1}(\gamma, q)$ cannot be parametrized in terms of an effective spreading rate λ_{PG_1} (see Fig. 3) whereas for fully Poissonian dynamics the mean transmissibility $T_{PP} = \lambda_{PP}/(1 + \lambda_{PP})$ only depends on the effective spreading rate $\lambda_{PP} = \beta/\gamma$ (see SI and Ref. [21]). However, if γ is small, we find that

$$\lim_{\gamma \rightarrow 0} \bar{T}_{PG_1}(\gamma, q) = \bar{T}_{PG_1}(\lambda_{PG_1}) = 1 - \lambda_{PG_1}^{-1}, \quad (9)$$

Thus, for sufficiently small values of q and γ (i.e., long mean infection and recovery times), the mean transmissibility $\bar{T}_{PG_1}(\gamma, q)$ only depends on the effective spreading rate λ_{PG_1} . In the SI, we show that this is also the case for the alternative formulation of Poisson-geometric SIR dynamics with ψ_{G_2} . A graphical interpretation of this result is that the phase separation lines in Fig. 3 merge as $\langle \tau \rangle_\phi = \gamma^{-1}$ and $\langle \tau \rangle_\psi$ tend to infinity.

To determine the relative size of the epidemic $S(\bar{T})$ as function of the mean transmissibility \bar{T} , we use a generating function approach and assume an uncorrelated network [21] (see SI for correlated networks):

$$S(\bar{T}) = 1 - G_0(u; \bar{T}), \quad (10)$$

where $u = G_1(u; \bar{T})$, $G_0(u; \bar{T}) = \sum_{k=0}^{\infty} P_k (1 - \bar{T} + u\bar{T})^k$, and

$$G_1(u; \bar{T}) = \frac{G'_0(u; \bar{T})}{G'_0(1; \bar{T})} = \frac{\sum_{k=0}^{\infty} P_k k (1 - \bar{T} + u\bar{T})^{k-1}}{\sum_{k=0}^{\infty} P_k k}. \quad (11)$$

The function $G_0(u; \bar{T})$ is the generating function of the distribution of occupied edges belonging to a certain node. The distribution of occupied edges leaving a node at which we arrived by following a randomly selected edge is generated by $G_1(u; \bar{T})$ and u is the probability that a node at the end of a randomly selected edge is occupied. Note that the generating function formalism is useful for cases when the exact network is unknown but only its degree distribution. For details on limitations of the described bond-percolation mapping, see Refs. [8, 26, 27].

As in Fig. 2, we now consider a random-regular graph with degree $k = 5$. The degree distribution is $P_k = \delta_{k5}$, where the Kronecker delta is $\delta_{kk'} = 1$ if $k = k'$ and zero otherwise. In Fig. 2, we show the analytical solution of Eqs. (10) and (11) for fully Poissonian (\bar{T}_{PP}) and Poisson-geometric (\bar{T}_{PG_1}) SIR dynamics. For a small number of initially infected nodes, the relative outbreak size $S(\bar{T})$ corresponds to the fraction of recovered nodes $\langle r \rangle$ (see Eq. (3)). We observe that the bond-percolation description of hybrid and fully geometric SIR (see top left panel of Fig. 4) outbreaks agree well with simulations.

Unifying non-Markovian SIR processes. Up to this point, we focused on hybrid SIR processes with variations in the infection-time distributions. To understand the general applicability of our simulation and analytical framework, we now consider non-Markovian SIR dynamics with recovery times that are distributed according to the Erlang distribution

$$\phi(\tau) = \frac{\gamma^n \tau^{n-1} e^{-\gamma\tau}}{(n-1)!}, \quad (12)$$

where n and γ are the so-called shape and rate parameters. The Erlang distribution allows us to account for recovery processes that are not just exponentially distributed but more concentrated within a certain time window. It is the distribution that describes the sum of n independent exponential variables with rate γ . The Erlang distribution has been used as an approximation of cell-cycle time distributions [28] and as such it is a better candidate for disease recovery processes as cells cycles have n stages through which they are progressing (e.g. $n = 4$ for COVID19 [29]). In Fig. 4 (top right), we observe that Erlang-geometric SIR processes can also not be described by an effective spreading rate. The considered examples of non-Markovian SIR processes show that the effective-spreading-rate description cannot uniquely characterize hybrid and general non-Markovian disease outbreaks. Instead, the mean transmissibility \bar{T} provides

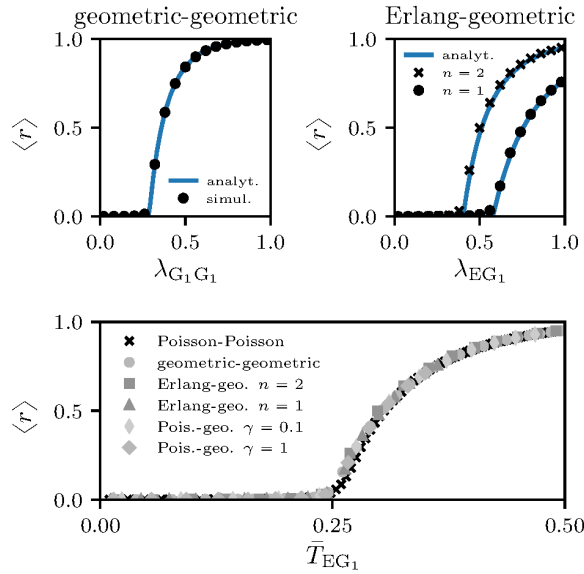


Figure 4. **Outbreak sizes for non-Markovian SIR processes.** In the top panels, we show the fraction of recovered nodes $\langle r \rangle$ (see Eq. (3)) as a function of the corresponding effective spreading rates. The bottom panel shows that different non-Markovian outbreak sizes collapse onto the same curve when plotted against \bar{T} . Numerical simulations have been performed for $N = 10^5$ nodes and $M = 10^2$ realizations with 100 random initial infections.

a unifying control parameter as we show in Fig. 4 (bottom). In the SI, we outline that this also holds for other networks.

Discussion and conclusion. We introduced numerical and analytical frameworks for the study of general (non-)Markovian SIR dynamics on networks. Furthermore, we proposed a novel hybrid SIR process that models infection and recovery as discrete-time Markovian and continuous-time non-Markovian processes, respectively. The discussed examples of hybrid SIR processes can account for cell-cycle distributions and latency intervals during which no infection events occur. We showed that the effective-spreading-rate description of Markovian SIR processes cannot uniquely capture the non-Markovian epidemic outbreaks anymore. However, our results suggest that the mean transmissibility provides a unifying description of (non-)Markovian SIR processes across a wide range of network structures (see SI for more details) and infection and recovery time distributions. This is of particular interest for disease control and hints at a (re-)definition of the epidemic threshold to appropriately account for disease dynamics and network structure [24]. Our work can contribute to more accurate and informative models of spreading processes on networks and meta-population spreading models [30, 31].

We thank J. Nagler for helpful comments. LB acknowledges financial support from SNF and Army Research Office (W911NF-18-1-0345) and N.A-F. financial support from SoBigData++ with grant agreement 871042.

L.B. and N.A-F. contributed equally to this work.

* lucasb@ethz.ch

† anino@ethz.ch

- [1] R. Pastor-Satorras, C. Castellano, P. Van Mieghem, and A. Vespignani, *Rev. Mod. Phys.* **87**, 925 (2015).
- [2] L. Böttcher, J. Nagler, and H. J. Herrmann, *Phys. Rev. Lett.* **118**, 088301 (2017).
- [3] N. Antulov-Fantulin, A. Lančić, T. Šmuc, H. Štefančić, and M. Šikić, *Phys. Rev. Lett.* **114**, 248701 (2015).
- [4] Y. Moreno, R. Pastor-Satorras, and A. Vespignani, *EPJ B* **26**, 521 (2002).
- [5] M. J. Keeling and P. Rohani, *Modeling infectious diseases in humans and animals* (Princeton University Press, 2011).
- [6] K. J. Sharkey, *Theor. Pop. Biol.* **79**, 115 (2011).
- [7] K. J. Sharkey, I. Z. Kiss, R. R. Wilkinson, and P. L. Simon, *Bull. Math. Biol.* **77**, 614 (2015).
- [8] B. Karrer and M. E. Newman, *Phys. Rev. E* **82**, 016101 (2010).
- [9] D. T. Gillespie, *J. Comp. Phys.* **22**, 403 (1976).
- [10] A.-L. Barabasi, *Nature* **435**, 207 (2005).
- [11] L. Böttcher, O. Woolley-Meza, and D. Brockmann, *PloS one* **12**, e0178062 (2017).
- [12] K.-I. Goh and A.-L. Barabási, *EPL* **81**, 48002 (2008).
- [13] M. Starnini, J. P. Gleeson, and M. Boguñá, *Phys. Rev. Lett.* **118**, 128301 (2017).
- [14] M. Boguñá, L. F. Lafuerza, R. Toral, and M. Á. Serrano, *Phys. Rev. E* **90**, 042108 (2014).
- [15] N. Masuda and L. E. Rocha, *SIAM Review* **60**, 95 (2018).
- [16] L. J. Allen, *Math. Biosci.* **124**, 83 (1994).
- [17] Z. Chen, *IEEE Access* **7**, 127669 (2019).
- [18] A. Clauset and N. Eagle, *arXiv:1211.7343* (2012).
- [19] J. Lessler, N. G. Reich, R. Brookmeyer, T. M. Perl, K. E. Nelson, and D. A. Cummings, *Lancet Infect. Dis.* **9**, 291 (2009).
- [20] P. Grassberger, *Math. Biosci.* **63**, 157 (1983).
- [21] M. E. Newman, *Phys. Rev. E* **66**, 016128 (2002).
- [22] P. G. Fennell, S. Melnik, and J. P. Gleeson, *Phys. Rev. E* **94**, 052125 (2016).
- [23] D. Tolić, K.-K. Kleineberg, and N. Antulov-Fantulin, *Sci. Rep.* **8**, 6562 (2018).
- [24] Q.-H. Liu, M. Ajelli, A. Aleta, S. Merler, Y. Moreno, and A. Vespignani, *Proc. Nat. Acad. Sci. USA* **115**, 12680 (2018).
- [25] M. L. Fredman and R. E. Tarjan, *JACM* **34**, 596 (1987).
- [26] E. Kenah and J. M. Robins, *Phys. Rev. E* **76**, 036113 (2007).
- [27] P. Trapman, *Theor. Pop. Biol.* **71**, 160 (2007).
- [28] C. A. Yates, M. J. Ford, and R. L. Mort, *Bull. Math. Biol.* **79**, 2905 (2017).
- [29] F. Pan, T. Ye, P. Sun, S. Gui, B. Liang, L. Li, D. Zheng, J. Wang, R. L. Hesketh, L. Yang, and C. Zheng, *Radiology* (2020), pMID: 32053470.
- [30] V. Colizza and A. Vespignani, *J. Theor. Biol.* **251**, 450 (2008).
- [31] W. Van den Broeck, C. Gioannini, B. Gonçalves, M. Quagiotto, V. Colizza, and A. Vespignani, *BMC Inf. Dis.* **11**, 37 (2011).